

Comparative Evaluation of Methods to Determine the Earth Pressure Distribution on Cylindrical Shafts: A Review

Tatiana Tobar¹ and Mohamed A. Meguid²

1. Tatiana Tobar, Graduate Student
Department of Civil Engineering and Applied Mechanics
McGill University, 817 Sherbrooke Street West
Montreal, Quebec, Canada H3A 2K6
Email: tatiana.tobarvalencia@mail.mcgill.ca

2. Mohamed A. Meguid*, Assistant Professor
Department of Civil Engineering and Applied Mechanics
McGill University, 817 Sherbrooke Street West
Montreal, Quebec, Canada H3A 2K6
Tel. (514) 398-1537 - Fax. (514) 398-7361
Email: mohamed.meguid@mcgill.ca
* Corresponding author

Abstract

Various methods used for calculating and measuring the earth pressure distribution on cylindrical shafts constructed in sand are evaluated. Emphasis is placed on a comparison between the calculated earth pressure using different methods for given sand and wall conditions. The effects of the assumptions made in developing these solutions on the pressure distribution are discussed. Physical modeling techniques used to simulate the interaction between vertical shafts and the surrounding soil are presented. The earth pressure measured and the wall movements required to establish active condition are assessed. Depending on the adopted method of analysis, the calculated earth pressure distribution on a vertical shaft lining may vary considerably. For shallow shafts, the theoretical solutions discussed in this study provide consistent estimates of the active earth pressure. As the shaft depth exceeds its diameter, the solutions become more sensitive to the ratio between the vertical and horizontal arching and only a range of earth pressure values can be obtained. No agreement has been reached among researchers as to the magnitude of wall movement required to establish active conditions around shafts and further investigations are therefore needed.

Keywords: Cylindrical shafts, earth pressure theory, physical modeling, soil-structure interaction.

1. Introduction

Vertical shafts are widely used as temporary or permanent earth retaining structures for different engineering applications (e.g. tunnels, pumping stations and hydroelectric projects). Determining the earth pressure acting on the shaft lining system is essential to a successful design. Classical earth pressure theories developed by Coulomb (1776) and Rankine (1857) have been often used to estimate earth pressure on shaft walls. These theories were originally developed for infinitely long walls under plane strain conditions. Terzaghi (1920) investigated the effect of wall movement on the magnitude of earth pressure acting on a rigid retaining wall. He concluded that for dense sand, a wall movement of about 0.1% of the wall height is necessary to reach the theoretical active earth pressure. Following from the work of Terzaghi (1920), extensive earth pressure research has been conducted (Terzaghi, 1934, 1954; Rowe, 1969; Bros, 1972; Sherif et al., 1982, 1984) to determine the wall displacement required for establishing the active stress state under two-dimensional conditions.

Several theoretical methods have been proposed for the calculation of the active earth pressure on cylindrical retaining walls supporting granular material (e.g. Berezantzev, 1958; Prater, 1977). However, the earth pressure distribution obtained using these methods was found to vary significantly. In addition, the required wall movement to reach the calculated pressures is yet to be understood.

Physical models have been used to measure the changes in earth pressure due to the installation of model shafts in granular material under normal gravity conditions or in a centrifuge. One of the key challenges in developing a model shaft is to simulate the radial movement of the

supported soil during construction. Researchers have developed different innovative techniques to capture these features either during or after the installation of an instrumented lining.

The objective of this study is to review some of the theoretical and experimental techniques to investigate the active earth pressure on cylindrical shaft linings installed in cohesionless ground. The assumptions made in developing different theoretical solutions and their effects on the calculated earth pressure are examined. Finally, a comparison is presented between different physical modeling techniques used to study the interaction between a shaft lining and the surrounding soil, and the measured earth pressure distributions are reproduced.

2. Theoretical Methods

When Coulomb (1776) and Rankine (1857) developed their two-dimensional earth pressure theories, they also established two simple methods of analysis: the limit equilibrium and the slip line method. Both methods are based on plastic equilibrium, however they differ in how the solution is obtained. The limit equilibrium method assumes a suitable failure surface, and basic statics is used to solve for the earth pressure. Conversely, the slip line method assumes the entire soil mass to be on the verge of failure, and the solution is obtained through a set of differential equations based on plastic equilibrium. Several attempts have been made to extend these methods to study the active earth pressure against cylindrical shafts in cohesionless media. Westergaard (1941) and Terzaghi (1943), proposed analytical solutions; Prater (1977) used the limit equilibrium method; and Berezantzev (1958), Cheng & Hu (2005), Cheng et al. (2007), Liu & Wang (2008), Liu et al. (2009) used the slip line method. In contrast to the classical earth pressure theories, where the active earth pressure calculated using the Coulomb or Rankine method are essentially the same, the distributions obtained for axisymmetric conditions may differ considerably depending on the chosen method of analysis, as discussed below.

2.1 Analytical Solutions

The earliest effort to investigate the state of stress around a cylindrical opening in soil was made by Westergaard (1941), who studied the stress conditions around small unlined drilled holes, based on the equilibrium of a slipping soil wedge. Terzaghi (1943) extended Westergaard's theory to large lined holes, thus proposed a method to calculate the minimum earth pressure exerted by cohesionless soil on vertical shafts liners. He determined the equilibrium of the sliding soil mass assuming $\sigma_\theta = \sigma_v = \sigma_l$ and $\sigma_r = \sigma_3$ inside the elastic zone and employing the Mohr-Coulomb yield criterion. Terzaghi obtained Equations 1 to 3 below for the lateral earth pressure on a shaft lining. As stated in Equation 3, Terzaghi proposed the use of a reduced angle of internal friction of the sand, ϕ^* , to account for the effect of the nonzero shear stresses in the solution.

$$m_\sigma = \frac{h}{a} \frac{N_\phi + 1}{2N_\phi} \frac{N_\phi - (N_\phi - 2)n_1^2}{N_\phi + n_1^{N_\phi+1}} \quad (1)$$

$$\tan \phi^* = \frac{n_1^2 - 1}{m_\sigma n_1^{N_\phi}} - \frac{2N_\phi}{N_\phi + 1} \frac{a}{h} \frac{n_1^{N_\phi+1} - 1}{n_1^{N_\phi}} \quad (2)$$

$$\phi^* = \phi - 5^\circ \quad (3)$$

where, $m_\sigma = p / \gamma a$, normalized earth pressure; $n_1 = r / a$, normalized extent of the yield zone; and $N_\phi = \tan^2 (45 + \phi^*/2)$; a = shaft radius; h = excavation depth; r = radial distance.

Fig. 1a shows the values of normalized earth pressure, m_σ , versus normalized depth, h/a , originally computed by Terzaghi (1943) for $\phi = 40^\circ$ and those computed by the authors for $\phi = 40^\circ$ and 41° . For $\phi = 40^\circ$ the difference between the calculated and original data is rather small. Increasing the friction angle from 40° to 41° causes a reduction in the normalized earth pressure

by approximately 9%. These numerical values were obtained using the reduced friction angle given by Eq. 3. The values of m_σ are computed from Eq. 2 for different assumed values of n_1 and the corresponding values of h/a are then computed from Eq. 1. The procedure is detailed by Terzaghi (1943).

Fig. 2 shows, among other solutions, the calculated earth pressure distribution with depth using the above equations for a shaft lining of radius, a , and height, h , installed in cohesionless soil with $\phi = 41^\circ$. The pressure generally increases with depth and reaches a normalized value, $p/\gamma a$, of 0.25 at a depth of approximately 5 times the shaft radius. For h/a greater than 5, the pressure increase is less significant and reaches a normalized value, $p/\gamma a$, of 0.30 at a depth of approximately 15 times the shaft radius.

2.2 Limit equilibrium

Prater (1977) adapted Coulomb wedge theory for axisymmetric conditions assuming a conical failure surface. He introduced into the analysis tangential and radial forces, T and F (See Fig. 1c). The force T is a function of the earth pressure coefficient on radial planes, λ , which is defined by the stress ratio σ_θ / σ_v . Prater argued that λ is a decisive parameter whose value should range between K_a and K_o and not equal to unity as was implicitly assumed by Terzaghi (1943). The earth pressure (force per unit length of the shaft circumference) P_1 is expressed by Eq. 4, where K_r is the coefficient of earth pressure for cylindrical shafts given by Eq. 5.

$$P_1 = 0.5 K_r \gamma h^2 \quad (4)$$

$$K_r = \frac{h}{a \tan \alpha} \tan(\alpha + \beta) \left(\frac{1}{3 \tan \alpha} - \frac{a}{h} \right) - \frac{\lambda}{3} \quad (5)$$

where, a = shaft radius; h = excavation depth; α = inclination of failure surface; β = angle between the reaction Q acting on the sliding body and the normal ($\beta = -\phi$ for active condition); λ = coefficient of lateral earth pressure on radial planes.

The earth pressure on the shaft is computed as follows. First the earth pressure, P_l , is computed at various depths, i.e. by incrementally increasing the depth. Second, the difference in force between successive increments is divided by the depth increment to obtain the average earth pressure for the increment. This average pressure is plotted versus depth as shown in Fig. 2. The values used in plotting Prater's solution in Fig 2 have been calculated using the above procedure ($\phi = 41^\circ$ and $\lambda = K_o$) in conjunction with the graphs presented by Prater (1977) to obtain the values of the coefficient K_r .

As shown in Fig. 2, Prater's method predicts a zero earth pressure at some depth below the surface; however, Prater recommended that the maximum earth pressure value should be used for design purposes.

2.3 Slip line method

Berezantzev (1958) extended the slip line method to calculate the earth pressure acting on cylindrical walls with horizontal backfill and uniform surcharge as shown in Fig.1b. To solve the equilibrium equations under axisymmetric conditions Berezantzev introduced into the analysis the Haar-Von Karman hypothesis which states that the hoop stress is equal to either the major or the minor principal stress (Yu, 2006). Thus, under active conditions Berezantzev assumed that inside the plastic zone the tangential and radial stresses are equal to the major and minor principal stresses, respectively, ($\sigma_\theta = \sigma_v = \sigma_1$ and $\sigma_r = \sigma_3$). Thus $\lambda = \sigma_\theta / \sigma_v = 1$. To simplify the calculations the slip lines were approximated to straight lines in the vertical direction and the

Mohr-Coulomb failure criterion was adopted. The governing equations took the form of two partial differential equations that he solved using the Sokolovski step-by-step computation method. Equation 6 gives the simplified form of the solution that evaluates the earth pressure on the shaft wall as reported by Fujii et al. (1994).

$$P_a = a \gamma \frac{\sqrt{K_a}}{\eta - 1} \left[1 - \frac{a}{r_b^{\eta-1}} \right] + q \left(\frac{a K_a}{r_b^\eta} \right) + \cot \phi \left[\left(\frac{a}{r_b^\eta} \right) K_a - 1 \right] c \quad (6)$$

where, $\eta = 2 \tan(\phi) \tan(45 + \phi/2)$; $r_b = a + h\sqrt{K_a}$; $K_a = \tan^2(45 - \phi/2)$; q = external surcharge; c = soil cohesion; a = shaft radius; h = excavation depth

As shown in Fig. 2, for a shaft of radius, a , in cohesionless soil and no external surcharge, q , the earth pressure distribution based on Berezantzev is similar to that calculated by Terzaghi, however the maximum pressure is smaller by approximately 40%.

Cheng & Hu (2005) extended Berezantzev's theory by modifying the Haar-Von Karman hypothesis, i.e. $\lambda = 1$, to develop a more general solution considering a variable earth pressure coefficient, λ . An expression for the active earth pressure was proposed as given below.

$$P_a = a \gamma \frac{\sqrt{K_a}}{\eta - 1} \left(1 - \frac{a}{r_b^{\eta-1}} \right) + q \frac{a K_a}{r_b^\eta} - \cot \phi \left[\frac{1 - \lambda + \eta}{\eta} - \frac{a \varepsilon}{r_b^\eta} K_a \right] c \quad (7)$$

where $\eta = \lambda \tan^2(45 + \phi/2) - 1$; $r_b = a + h\sqrt{K_a}$; $\varepsilon = (1 - \lambda)\eta^{-1} \tan^2(45 + \phi/2) + 1$; $0 < \eta < 1$ and $\phi \neq 0$.

Cheng and Hu (2005) found that the case of $\lambda = 1$ produces the lowest lateral pressure and therefore a value of $\lambda = K_o = (1 - \sin \phi)$ was suggested for engineering applications. The upper

and lower bounds of the lateral earth pressure can then be obtained using $\lambda = K_o$ and $\lambda = 1$, respectively, as shown in Fig. 2 ($c = 0$ and $q = 0$).

Cheng et al. (2007) and Liu & Wang (2008) introduced additional parameters into the analysis including wall friction, backfill slope, surcharge loads and soil cohesion. Solution of the characteristic equations was obtained numerically leading to a lengthy set of expressions that are omitted in this review. The results indicated that the pressure distribution is consistently smaller than the one obtained using the simplified solution of Cheng & Hu (2005). Liu & Wang (2008) examined the effect of wall inclination and developed a solution that was essentially similar to that obtained by Cheng & Hu (2005) simplified solution. They concluded that the analytical solution presented by Cheng & Hu provides a reasonable estimate of the active pressure on a vertical shaft for horizontal backfill material and zero wall friction.

Liu et al. (2009) further extended Berezantzev's theory by assuming a linearly varying λ such that it decreases across the plastic zone from unity at the shaft circumference to K_o at the elasto-plastic interface. The results obtained based on this method were found to agree with those previously reported by Cheng et al. (2007).

Based on the above studies it can be concluded that, for axisymmetric excavations under active conditions, there exist two coefficients of lateral earth pressure: one defined as the ratio of radial stresses acting on circumferential planes, $K = \sigma_r / \sigma_v$; and the second defined as the ratio of tangential stresses acting on radial planes, $\lambda = \sigma_\theta / \sigma_v$. In other words, during shaft construction the initial stresses redistribute such that the value of K decreases until it reaches K_a , while the value of λ increases such that $K_a < K_o < \lambda$. Therefore, the coefficient λ provides a measure of the horizontal arching that has occurred in the soil adjoining the excavation.

2.4 Comparison between different theoretical solutions

A summary of the earth pressure distribution calculated using some of the above methods for a given shaft geometry (height, h and radius, a) and soil property (ϕ) is presented in Fig. 2. Although all methods predict pressures that are less than the at-rest and active values, the distributions of earth pressure with depth notably differ. The Terzaghi and Berezantzev methods implicitly assume λ equals unity, leading to a minimum value of the active earth pressure. This is consistent with the results of the plastic equilibrium and slip line methods. Both solutions result in pressure distributions that ultimately reach a constant earth pressure at some depth below surface. As discussed earlier, Prater's method predicts a different pressure distribution that can be characterized (for the same shaft geometry and soil conditions) by a rapid increase in pressure up to a depth of about 4.5 times the shaft radius and then a decrease to zero at a depth of 8.5 times the shaft radius. The solution of Cheng & Hu provided the lower and upper bounds of the lateral earth pressure as given by $\lambda = 1$ and $\lambda = K_o$, respectively. For $\lambda = 1$ the earth pressure is the same as that calculated using the Berezantzev method. Fig. 2 shows that for shallow shafts, where the shaft height ranges from 1 to 2 times the shaft radius, the difference between the above theoretical methods is insignificant.

3. Experimental Investigations

Several studies have been conducted to measure the earth pressure distribution due to the installation of a model shaft in granular material. To simulate the lining installation and the radial soil movement during construction, different techniques have been developed that can be grouped into three main categories: (a) shaft sinking; (b) temporary stabilization of the excavation using fluid pressure (liquid or gas); and (c) the use of a mechanically adjustable

lining. These techniques are briefly described and samples of the experimental results are presented.

3.1 Shaft sinking

The sinking technique consists of advancing a small model caisson equipped with a cutting edge at a recess distance, S , from the lining surface. This recess S is used to simulate the induced soil movement during construction. Walz (1973) investigated the lateral earth pressure against circular shafts using the above technique. The shaft lining consisted of a 105 mm diameter and 630 mm deep tube composed of twelve steel rings and a cutting edge ring equipped with recess, S , ranging from 0 to 5 mm, as shown in Fig. 3a. The soil container used was a cylindrical tub of 1 m diameter and 1 m deep filled with dry sand. Prior to the filling process, a hollow tube of small diameter was installed vertically across the container. This tube was attached to the cutting edge ring at the soil surface, and then pulled down using a motor to sink the model shaft. As the shaft was advanced into the soil, the soil cutting was directed through the vertical tube out of the container. Each lining ring was divided into three equal segments that were kept in position using z-shaped aluminum arms attached to a central piece as shown in Fig. 3a. These z-shaped pieces were equipped with strain gauges, and the entire system was calibrated to directly read the earth pressure acting against the lining. The normalized earth pressure distribution versus normalized depth for $S = 0$ and 2 mm are shown in Fig. 3b. The introduction of the 2 mm recess has lead to a significant decrease in the measured earth pressure along the lining, with a maximum reduction of about 75% at $h/a = 0.5$.

3.2 Temporary stabilization using fluid pressure

In this technique, the soil to be excavated is replaced by a flexible rubber bag filled with liquid or gas. The liquid level, or gas pressure, is reduced in stages to simulate the shaft excavation process. This technique is generally used in centrifuge testing due to the restrictions in modeling excavation during the test.

Lade et al. (1981) conducted a series of centrifuge tests to investigate the lateral earth pressure against shafts in sand. A cylindrical tub of 850 mm diameter and 695 mm deep was used as the test container in which dry fine Leighton Buzzard sand ($\gamma = 15.35$ to 15.5 kN/m^3 , $\phi = 38.3^\circ$) was placed by pluvial deposition. The lining was formed using a 0.35 mm thick Melinex sheet. The soil inside the shaft was replaced by two different liquids: ZnCl_2 -solution with density similar to that of the soil and paraffin oil with a density of 7.65 kN/m^3 . The excavation process was modelled by removing the liquid in four stages and the liquid level was monitored. The readings of eight strain gauge sets installed along the lining were recorded and used to calculate the lateral earth pressure. Earth pressure cells and LVDT's were used to monitor the stresses around the shaft and the surface settlement, respectively. An overview of the test setup is shown in Fig. 4. The radial strains in the lining and the normalized earth pressures versus normalized depth are reproduced in Fig. 5. Large inward movements at the base of the fully excavated shaft were recorded which corresponded to large pressures at this depth. Before the fluid removal, expansion of the shaft lining was observed due to larger pressures exerted by the liquid inside the shaft than the outside soil. Similar observations were made by Kusakabe et al. (1985) in a series of centrifuge tests conducted to investigate the influence of axisymmetric excavation on buried pipes. Fig. 5 further shows that the measured pressures are higher than the calculated using Berezantzev method.

Konig et al. (1991) carried out a series of centrifuge tests to study the effects of the shaft face advance on a pre-installed lining. The model shaft consisted of two sections: an upper section made of rigid tube to simulate the installed lining, and a lower section made of rubber membrane to model the unsupported area of the excavation. At the initial condition, the membrane was pressurized with air to equilibrate the pressure exerted by the soil. To simulate the shaft face advance, the air pressure was incrementally reduced. The lateral movement of the rubber membrane was monitored using LVDT's embedded in the sand; the stresses in the shaft lining were monitored using strain gauges installed at different distances from the end of the lining. Results indicated that for dry sand, only a small support pressure was needed to maintain stability. However, there was a significant load transfer to the lining closest to the excavation face due to arching and stress redistribution in the soil.

3.3 Mechanically adjustable lining

In this technique, a mechanical system is used to move a rigid shaft lining in order to simulate the soil displacement that may occur during the excavation process. Using this technique, it is possible to impose a homogeneous radial displacement along the entire shaft height at a controlled rate. However, the mechanism required to model the inward movement of the shaft lining is challenging. Researchers have adopted simplified models to simulate the radial displacement of the lining (Fujii et al., 1994; Imamura et al., 1999), or took advantage of the radial symmetry to model only a portion of the problem (Herten & Pulsfort, 1999; Chun & Shin, 2006). Tobar & Meguid (2009) developed a mechanical system that allowed for the modeling of both the full shaft geometry as well as the radial displacement of the lining.

Using a mechanically adjustable shaft model, Fujii et al. (1994) conducted centrifuge tests to study the effects of wall friction and soil displacements on the earth pressure distribution around

rigid shafts. The lining was made of an aluminum cylinder of 60 mm in diameter split vertically into two semi-cylinders; one-half was instrumented with small stress transducers and horizontally moved using a motor to simulate the radial displacement of the shaft lining. Details of the apparatus are shown in Fig. 6a. The model shaft was placed into a rectangular soil container and Toyoura dry sand was rained around it up to 200 mm in height, H . Four tests were conducted for different densities and wall friction conditions. The measured earth pressure versus normalized depth for dense sand ($\phi = 42^\circ$, $\gamma = 14.7 \text{ kN/m}^3$) and different wall friction is shown in Fig. 6b along with the earth pressure calculated from Berezantzev method. The experimental results show good agreement with the theoretical solution of Berezantzev (1958). Little change in the measured earth pressure was reported at displacements greater than 1% of the wall height, H (6.6% of the shaft radius), and the wall friction was found to have a negligible effect on the measured earth pressure distribution.

Imamura et al. (1999) developed a model shaft similar to that used by Fujii et al. (1994). However, the instrumented semi-cylinder was horizontally translated using an external mechanism attached to a motor. Air-dried Toyoura sand with $\phi = 42^\circ$ and $\gamma = 15.2 \text{ kN/m}^3$ was used during the four centrifuge tests conducted to study the development of the active earth pressure around shafts and the extent of the yield zone. They concluded that the earth pressure decreases with increasing wall displacement until it coincides with Berezantzev's solution at a wall displacement that corresponds to 0.2% of the wall height, H (1.6% of the shaft radius). The maximum extent of the yield zone was found to be approximately 0.7 times the shaft diameter.

Herten & Pulsfort (1999) took advantage of the radial symmetry of the problem and modeled only one quadrant of the shaft. The test setup consisted of one quarter of a cylindrical shaft with 0.4 m in diameter and 1 m long. The model shaft was placed along one corner of a rectangular

box of 1 x 1 m in plan and 1.2 m in height. To minimize the wall friction, the walls were lubricated using Teflon film and oil. The test container was filled using pluvial deposition with dry fine sand of $\phi = 41^\circ$ in dense state (36% porosity). The shaft lining was horizontally moved using a motor to simulate the radial displacement of the shaft. Details of the test setup and the results of one of the four tests conducted are shown in Fig. 7. Little change in the measured lateral earth pressure occurred for wall displacements greater than 0.05% of the wall height (0.25% of the shaft radius).

Chun & Shin (2006) conducted model tests to study the effects of wall displacement and shaft size on the earth pressure distribution using a mechanically adjustable semi-circular shaft. The lining was made from an acrylic semi-cylinder that was cut longitudinally into three equal segments, i.e. each span an angle of 60° , to accommodate the changes in diameter during testing. Transversally the shaft was divided into five equal segments; some of them were used as sensitive areas for load cells installed behind the lining. Fig. 8a shows a schematic of the model.

The soil container used was a rectangular box, 0.7 m wide, 1 m long and 0.75 m deep filled with dry sand ($\phi = 41.6^\circ$; $\gamma = 16.4 \text{ kN/m}^3$; $D_r = 81\%$). Three different shaft radii, a , equal to 0.175, 0.15 and 0.115 m, and a constant depth, $H = 0.75 \text{ m}$, were tested. The reported earth pressure versus depth at various wall displacements for a smooth shaft and aspect ratio, H/a , equal to 4.286 are presented in Fig. 8b. The results indicate that earth pressure decreased with increasing wall movement and became minimum when the wall movement reached 0.6 to 1.8% of the wall height. In Fig. 8 the earth pressure calculated from Berezantzev and Terzaghi methods are shown for comparison. It appears from this comparison that the measured earth pressures are higher than that predicted from Berezantzev; Terzaghi's distribution falls between the measured earth pressure at S equal to 0.43 and 1.87 mm (0.06% and 0.25% of the wall height, H). Chun & Shin

(2006) found that soil failure extended a distance of approximately one shaft radius from the outer perimeter of the lining.

Tobar & Meguid (2009) conducted a series of tests under normal gravity to investigate the changes in lateral earth pressure due to radial displacement of the shaft lining. The developed apparatus allowed for the modeling of both the full geometry of the shaft and the radial displacement of the lining. It was built using six curved lining segments held vertically using segment holders (Fig. 9a). A simple mechanism was developed to translate the lining segments radially; it consisted mainly of steel hinges that connected the segment holders to central nuts. These nuts pass through a central threaded rod extended along the shaft axis. As the axial rod was rotated, the nuts moved vertically, pulling the segment holders radially inwards and consequently the shaft lining was uniformly translated.

The model shaft (0.15 m in diameter and 1 m long) was placed into a circular container of 1.22 m diameter and 1.07 m depth. The container was filled with coarse dry sand ($\phi = 41^\circ$; $\gamma = 14.7$ kN/m³) using pluvial deposition. The axisymmetric active earth pressure fully developed when the wall displacements, S , ranged between 0.2% and 0.3% of the wall height, H . It was concluded that for $S \geq 0.1\% H$, the measured pressures fell into the range predicted by Cheng & Hu (2005); and that at $S \geq 0.3\% H$, the measured pressures closely followed the pressure distributions calculated using Terzaghi (1943) and Berezantzev (1958) methods.

3.4 Discussion of experimental investigations

Table 1 shows a summary of the required wall displacement for establishing active conditions. To simplify the design and operation of the shaft models, simplified mechanisms were used to reduce the shaft diameter uniformly. It is evident that no agreement has been reached among

researchers as to the required wall movement to reach active conditions. The displacement ranged from 0.05% to 1.8% of the shaft height as shown in Table 1. This can be attributed to the difference in the testing conditions, shaft geometry, and wall movement technique used in each study. It is therefore recommended that large-scale experiments be conducted using full shaft geometry to account for the gravity effects and confirm these conclusions. Table 2 presents the advantages and disadvantages of the experimental techniques discussed in the previous section.

4. Conclusions

A comparative study of the theoretical and experimental methods used to determine the earth pressure on cylindrical shafts has been presented. For shallow shafts ($H \leq 2a$), the theoretical solutions provide approximate estimates of the active earth pressure distribution. As the shaft depth exceeds its diameter, the solutions become more sensitive to the ratio between the vertical and horizontal arching and therefore only a range of earth pressure values can be calculated. No agreement has been reached among researchers as to the magnitude of wall movement required to establish active conditions around the shaft and further investigations are therefore needed.

Acknowledgements

This research is supported by the Natural Sciences and Engineering Research Council of Canada (NSERC) under grant number 311971-06.

References

- Berezantzev, V.G. 1958. Earth pressure on the cylindrical retaining walls. *Conference on earthpressure problems*. Brussels, pp 21-27.
- Bros, B. 1972. The influence of model retaining wall displacements on active and passive earth pressure in sand. *Proc. 5th European Conf. on Soil Mech. Found. Eng*, Madrid, Vol. 1, pp. 241-249.

Cheng, Y.M., and Hu, Y.Y. 2005. Active earth pressure on circular shaft lining obtained by simplified slip line solution with general tangential stress coefficient. *Chinese Journal of Geotechnical Engineering*, 27 (1), 110-115.

Cheng, Y. M., Hu, Y.Y and Wei W. B. 2007. General axisymmetric active earth pressure by method of characteristics-Theory and numerical formulation. *International Journal of Geomechanics*, 7 (1), 1-15.

Chun, B, and Shin, Y. 2006. Active earth pressure acting on the cylindrical retaining wall of a shaft. *South Korea Ground and Environmental Engineering Journal*, 7 (4), 15-24.

Coulomb C.A., 1776. Essai sur une application des regles des maximis et minimis a quelques problemes de statique relatifs a l'architecture. Memoires de Mathématique et de Physique, Présentés a l'Académie Royale des sciences, par divers Savants, et lûs dans ses Assemblées, Paris, Vol. 7, (volume for 1773 published in 1776), pp. 343-382

Fujii, T., Hagiwara, T., Ueno, K. and Taguchi, A. 1994 Experiment and analysis of earth pressure on an axisymmetric shaft in sand. *Proceedings of the 1994 International Conference on Centrifuge*, Singapore, p 791-796.

Herten, M., and Pulsfort, M. 1999. Determination of spatial earth pressure on circular shaft constructions. *Granular Matter*, 2 (1), 1-7.

Imamura, S., Nomoto, T., Fujii, T., and Hagiwara, T. 1999 "Earth pressures acting on a deep shaft and the movements of adjacent ground in sand," In: O. Kusakabe, K. Fujita, and Y. Miyazaki, Eds., *Proceedings of the international symposium on geotechnical aspects of underground construction in soft ground*. Tokyo, Japan: Balkema, Rotterdam, pp 647-652.

Konig, D., Guettler, U., and Jessberger, H.L. 1991. Stress redistributions during tunnel and shaft constructions. *Proceedings of the International Conference Centrifuge 1991*, Boulder, Colorado, pp 129-135

Kusakabe, O., Tsutomu, K., Akira O., Nobuo, T., and Nobuaki, N. 1985. Centrifuge model test on the influence of axisymmetric excavation on buried pipes. *Proceedings of the 3rd international conference ground movements and structures*: Pentech Press, London, England, pp 113-128.

Lade, P.V., Jessberger, H.L., Makowski, E., and Jordan, P. 1981. Modeling of deep shafts in centrifuge test. *Proceedings of the International Conference on Soil Mechanics and Foundation Engineering*, Stockholm, Sweden, Vol. 1, pp 683-691.

Liu, F.Q., and Wang, J.H. 2008. A generalized slip line solution to the active earth pressure on circular retaining walls, *Computers and Geotechnics*, 35 (2), 155-164.

- Liu, F.Q., Wang, J.H., and Zhang, L.L. 2009. Axi-symmetric active earth pressure obtained by the slip line method with a general tangential stress coefficient. *Computers and Geotechnics*, 36 (1-2), 352-358.
- Prater, E.G. 1977. Examination of some theories of earth pressure on shaft linings. *Canadian Geotechnical Journal*, 14 (1), 91-106.
- Rankine, W.J.M. 1857 On the stability of loose earth, *Philosophical Transactions of the Royal Society of London*, 147, 9-27.
- Rowe, P.W. 1969. Progressive failure and strength of sand mass. *Seventh Intern Conf. on Soil Mech. and Found. Engr.*, Vol. 1., pp. 341-349
- Sherif, M.A., Fang, Y.S. and Sherif, R 1984. K_a and K_o behind rotating and non-yielding walls. *Journal of Geotechnical Engineering*, 110 (1), 41-56.
- Sherif, M.A., Ishibashi, I., and Lee, C.D. 1982 "Earth pressures against rigid retaining walls," *American Society of Civil Engineers, Journal of the Geotechnical Engineering Division*, Vol. 108, No. GT5, pp 679-695.
- Terzaghi, K. 1920. Old earth-pressure theories and new test results. *Engineering News-Record*, 85 (13), 632-637.
- Terzaghi, K. 1934. Large retaining-wall tests. *Engineering News-Record*. 112 (5), 23.
- Terzaghi, K. 1943. Theoretical soil mechanics, New York: John Wiley & Sons.
- Terzaghi, K. 1953. Anchored bulkheads. *American Society of Civil Engineers Proceedings, ASCE*, Vol. 79, p 39.
- Tobar, T. and Meguid, M.A. 2009. Distribution of earth pressure on vertical shafts. 62nd Canadian Geotechnical Conference, Halifax, September 2009, CD, 6 pages.
- Walz, B. 1973. Left bracket apparatus for measuring the three-dimensional active soil pressure on a round model caisson right bracket. *Baumaschine und Bautechnik*, 20 (9), 339-344. (In German)
- Westergaard, H.M. 1941. Plastic state of stress around deep well. *Civil Engineering (London)*, 36(421), pp 527-528.
- Yu, H.S. 2006. Plasticity and Geotechnics: Springer, pp 326

Nomenclature

A	Shaft radius
C	Soil cohesion
D_r	Relative density
F	Radial force
G	Gravitational constant of the Earth
G_s	Specific gravity
H	Excavation depth measured from ground surface
H	Shaft wall height
K	Coefficient of lateral earth pressure on circumferential planes, $K = \sigma_\theta / \sigma_v$
K_a	Coefficient of earth pressure at active conditions, $K_a = \tan^2(45 - \phi/2)$
K_o	Coefficient of earth pressure at rest
K_r	Coefficient of earth pressure for cylindrical shafts
m_σ	Normalized earth pressure, $m_\sigma = p / \gamma a$
$N = N_\phi =$	$\tan^2(45 + \phi/2)$
n_l	Normalized extent of the yield zone, $n_l = r / a$
$P = p$	Lateral earth pressure
p_a	Active earth pressure
P_o	Lateral earth pressure at $S = 0$ mm
P_l	Earth pressure force per unit length of the shaft circumference
Q	External surcharge
R	Radial distance
S	Radial displacement at shaft wall or radial soil movement at soil-wall interface

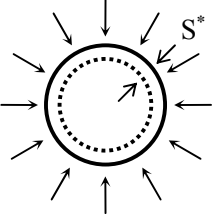
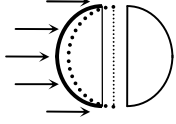
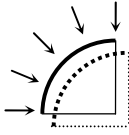
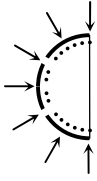
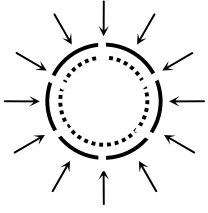
T	Tangential force
W	Weight of the soil wedge
α	Inclination of the failure surface
β	Angle between the reaction Q acting on the sliding body and the normal
Γ	Unit weight
Δ	Friction angle
λ	Coefficient of lateral earth pressure on radial planes, ($\lambda = \sigma_{\theta} / \sigma_v$)
$\sigma_1, \sigma_2, \sigma_3$	Major, intermediate and minor principal stresses
σ_r	Radial stress
σ_{θ}	Tangential stress
σ_v	Vertical stress
ϕ	Angle of internal friction of the soil
ϕ^*	Reduced angle of internal friction, $\phi^* = \phi - 5^\circ$

List of Tables

Table 1. Comparison of the required wall displacements for active condition

Table 2. Advantages and disadvantages of selected shaft modeling technique

Table 1. Comparison of the required wall displacements for active condition

Prototype	Model	Required wall movement (S) to reach active condition	Soil
	Semi-cylinder (non-segmented) 	<ul style="list-style-type: none"> Fujii et al. (1994) $S \geq 1\% H^{**}$ or $S \geq 6.6\% a^{***}$ Imamura et al. (1999) $S = 0.2\% H$ or $S = 1.6\% a$ 	Dense sand
	Quarter cylinder (non-segmented) 	<ul style="list-style-type: none"> Herten and Pulsfort (1999) $S = 0.05\% H$ or $S = 0.25\% a$ 	Dense sand
	Semi-cylinder (Segmented) 	<ul style="list-style-type: none"> Chun and Shin (2006) $0.6\% H < S < 1.8\% H$ or $0.15\% a < S < 0.4\% a$ 	Dense sand
	Full cylinder (Segmented) 	<ul style="list-style-type: none"> Tobar and Meguid (2009) $S \geq 0.2\% H$ or $S \geq 2.5\% a$ 	Loose sand

* Radial wall displacement; ** Wall height; *** Shaft radius

Table 2. Advantages and disadvantages of selected shaft modeling technique

Method	Advantages	Disadvantages
Shaft Sinking	<ul style="list-style-type: none"> • Suitable for modeling shafts constructed using the sinking technique. 	<ul style="list-style-type: none"> • Causes soil disturbance. • High shear stresses can develop along the shaft. • Difficult to assess the effects of the shear stresses along the wall on the lateral earth pressure.
Pressurized Bags	<ul style="list-style-type: none"> • Can be used to simulate shaft excavation under 1g and in a centrifuge. 	<ul style="list-style-type: none"> • Applicable for flexible shaft linings.
Liquid bag	<ul style="list-style-type: none"> • Simplifies modeling initial stress state in centrifuge. • Can simulate the excavation advance process. 	<ul style="list-style-type: none"> • The liquid inside the bag may exert more pressure in the centrifuge than the soil outside. • Large inward deformation may occur at the base of the excavation.
Air bag	<ul style="list-style-type: none"> • Flexibility to readjust air pressure during testing. • Suitable for modeling small sections of the excavation. 	<ul style="list-style-type: none"> • The pressure imposed along the model shaft is based on average theoretical value. • Does not simulate the excavation advance.
Mechanically Adjustable Lining	<ul style="list-style-type: none"> • Easy to model the translation displacement of the shaft wall. • Can be used under 1g or in a centrifuge. • Facilitates the installation of pressure cells behind the lining. 	<ul style="list-style-type: none"> • Limited to rigid lining models. • Involves oversimplification of the geometry or the radial displacement of the soil around the shaft. • Does not simulate the excavation advance.

List of Figures

Fig.1. (a) Earth pressure distributions using Terzaghi method for $\phi = 40^\circ$ and 41° (b) Earth Pressure acting on a cylindrical retaining wall as studied by Berezantzev (1958) . (c) Failure surface assumed by Prater (1977)

Fig. 2. Earth pressure distributions a shaft of depth h , radius a in cohesionless soil and no surcharge

Fig. 3. Model shaft used in the shaft-sinking method and the measured earth pressure distribution (Adapted from Walz, 1973).

Fig. 4. Test setup used in the fluid pressure technique (Adapted from Lade et. al., 1981).

Fig. 5. Radial strains and the corresponding earth pressure distributions (Adapted from Lade et al., 1981).

Fig. 6. Semi-cylindrical model shaft and earth pressure distribution for smooth and rough walls (Adapted from Fujii et al., 1994).

Fig. 7. Quarter-cylinder model shaft and the earth pressure distribution (Adapted from Herten & Pulsfort, 1999).

Fig. 8. Semi-cylindrical model shaft and the measured earth pressure using a shape aspect ratio, H/a , of 4.286 (Adapted from Chun & Shin, 2006).

Fig. 9. Details of the full axisymmetric shaft apparatus and the measured results (Tobar & Meguid, 2009).

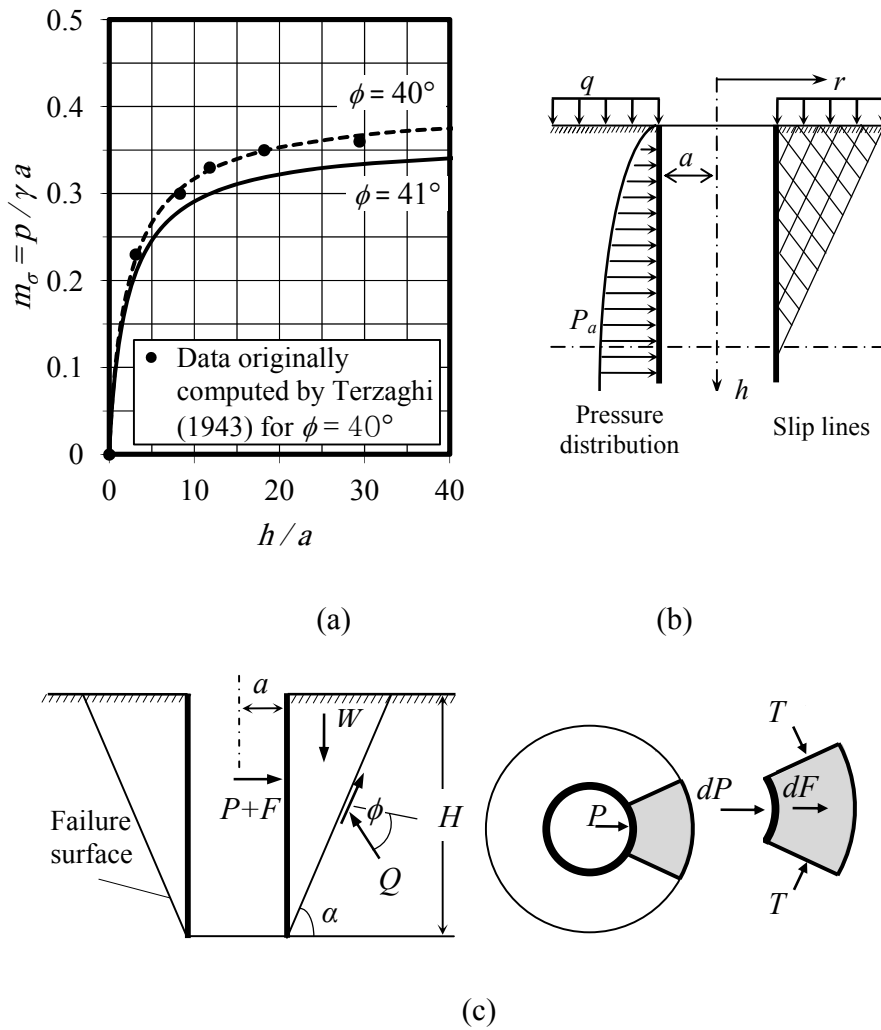


Fig.1. (a) Earth pressure distributions using Terzaghi (1943) for $\phi = 40^\circ$ and 41°
 (b) Earth Pressure acting on a cylindrical retaining wall as proposed by Berezantzev (1958) (c) Failure surface assumed by Prater (1977)

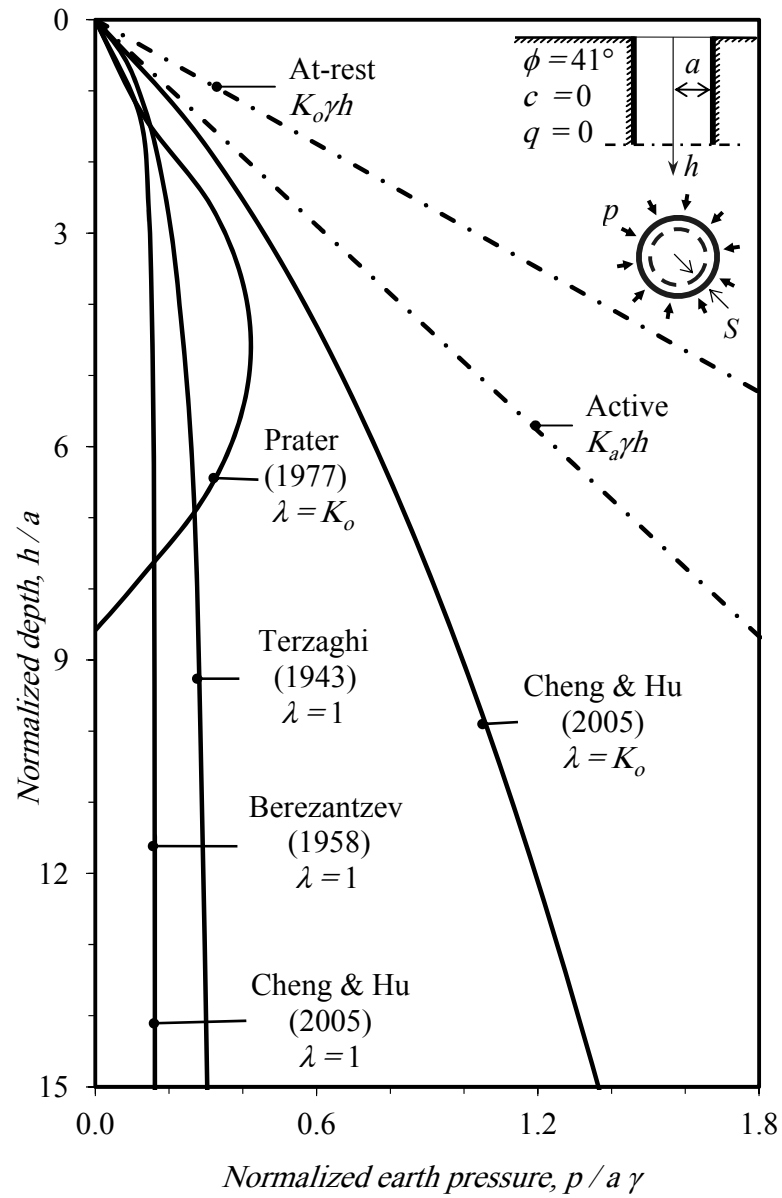
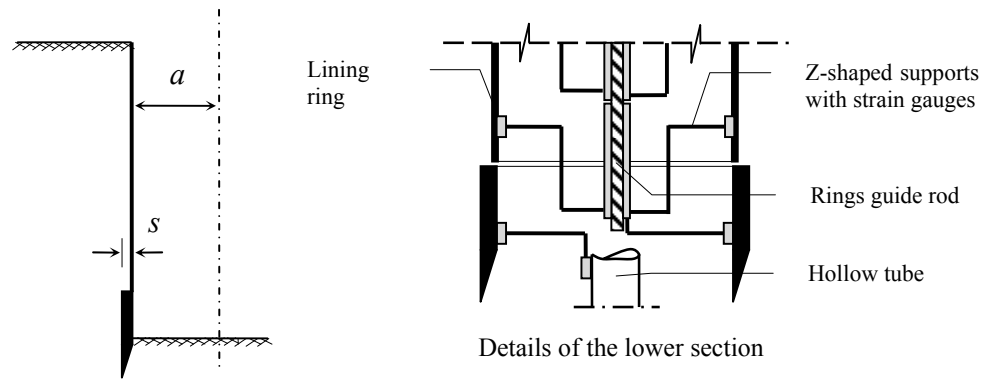
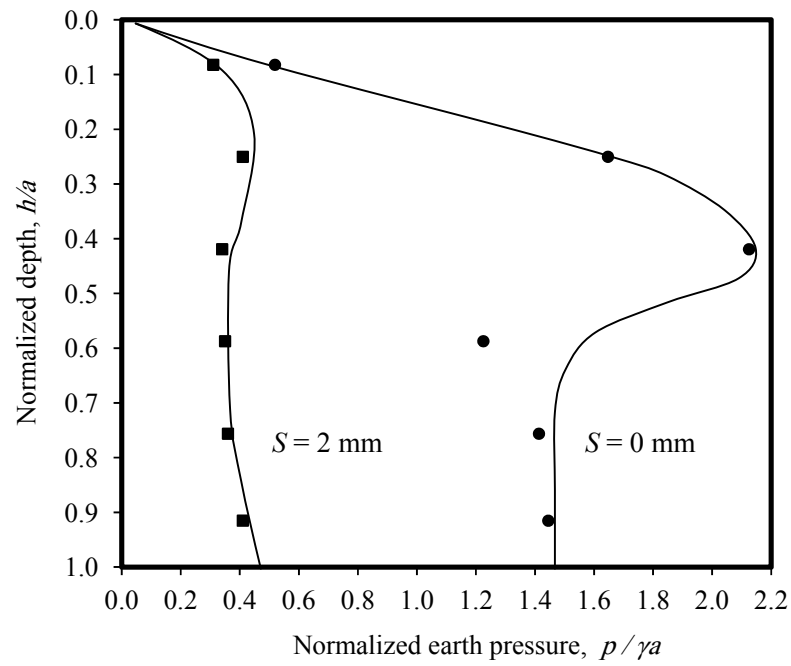


Fig. 2. Earth pressure distributions on a shaft of depth h , radius a , in cohesionless soil and no surcharge



a) Schematic of the model shaft



b) Experimental results

Fig. 3. Model shaft used in the shaft-sinking method and the measured earth pressure distribution (Adapted from Walz, 1973)

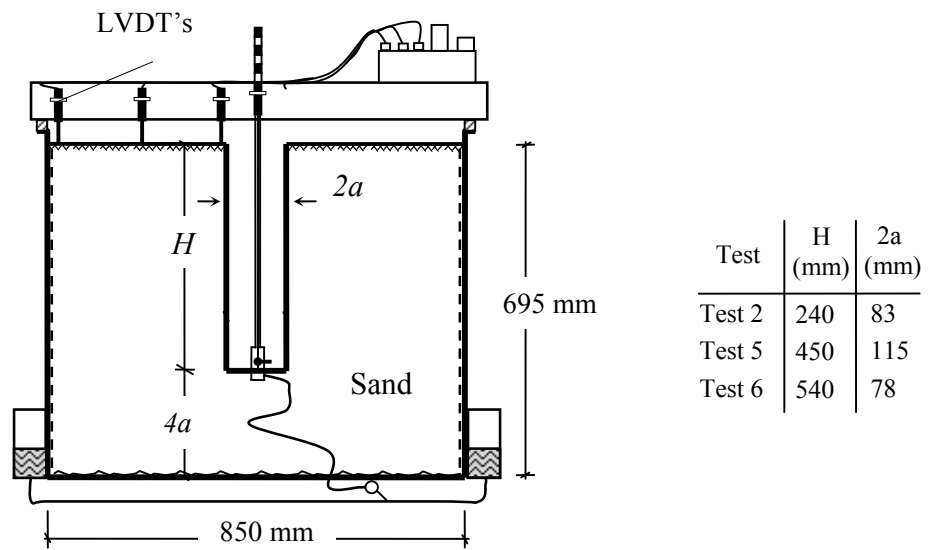
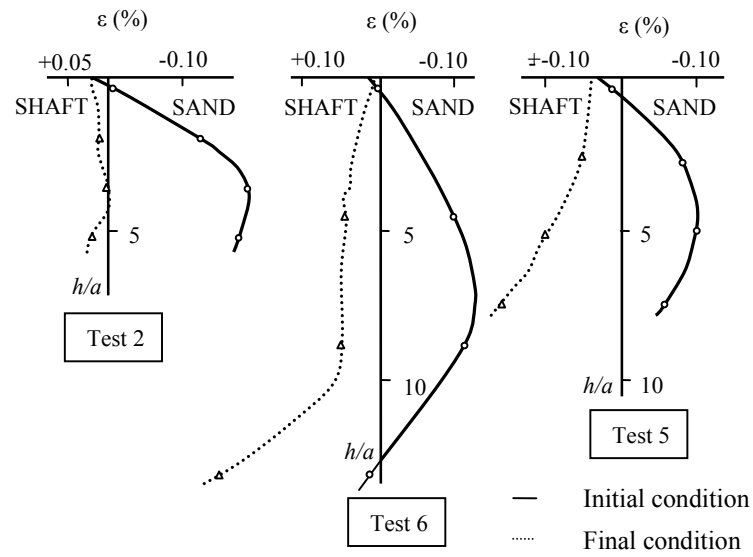


Fig. 4. Test setup used in the fluid pressure technique (Adapted from Lade et. al., 1981)



a) Radial strains in the lining

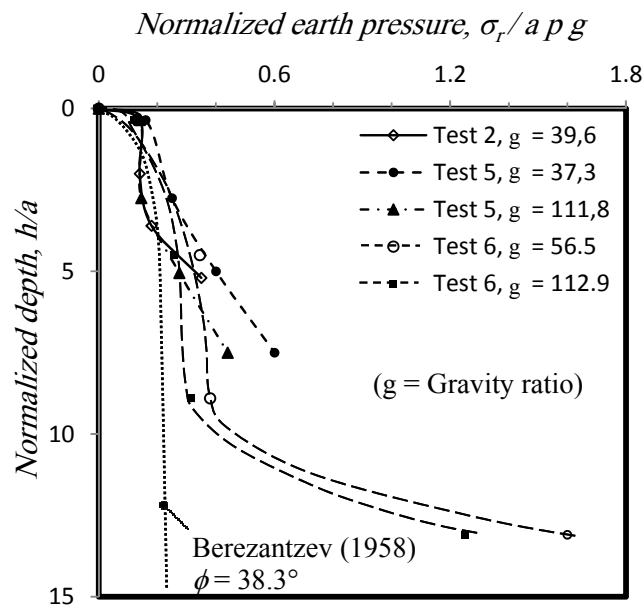
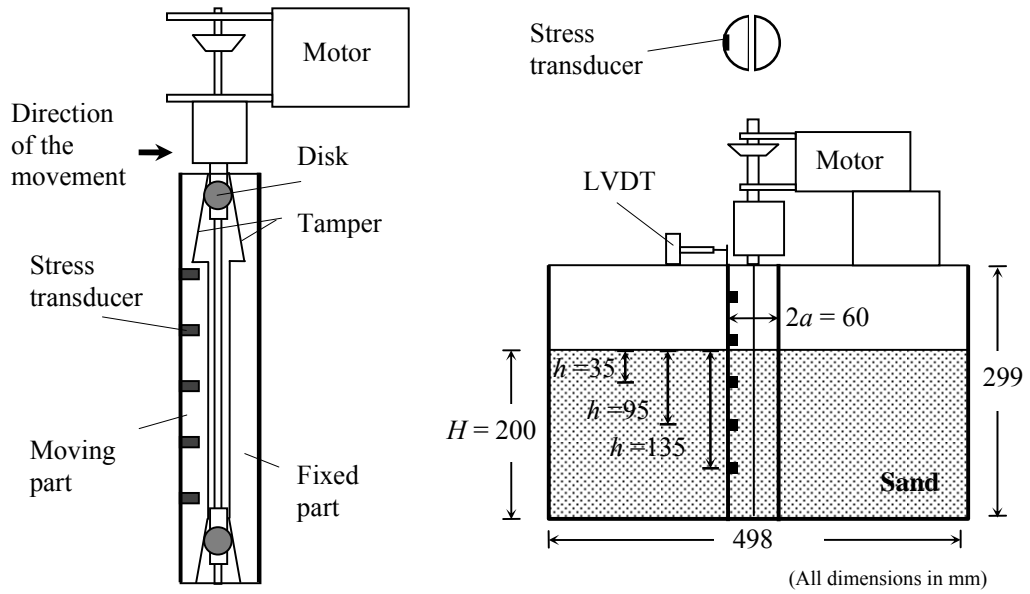
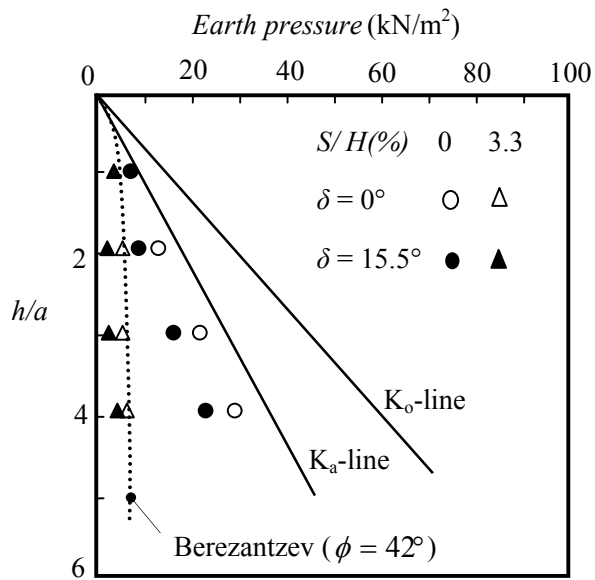


Fig. 5. Radial strains and the corresponding earth pressure distributions (Adapted from Lade et al., 1981)

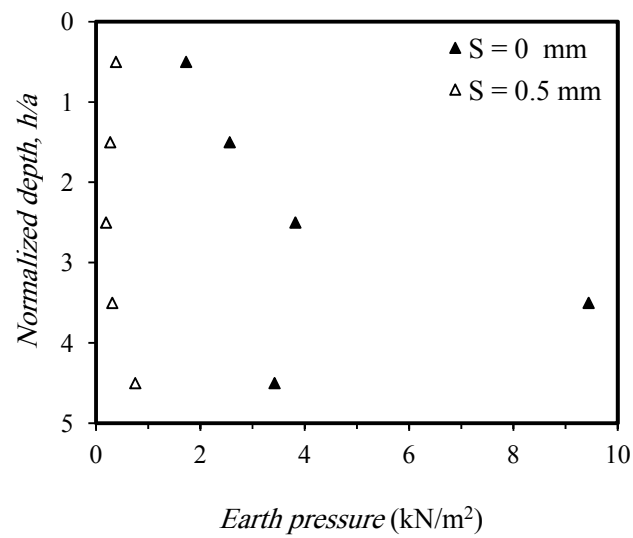
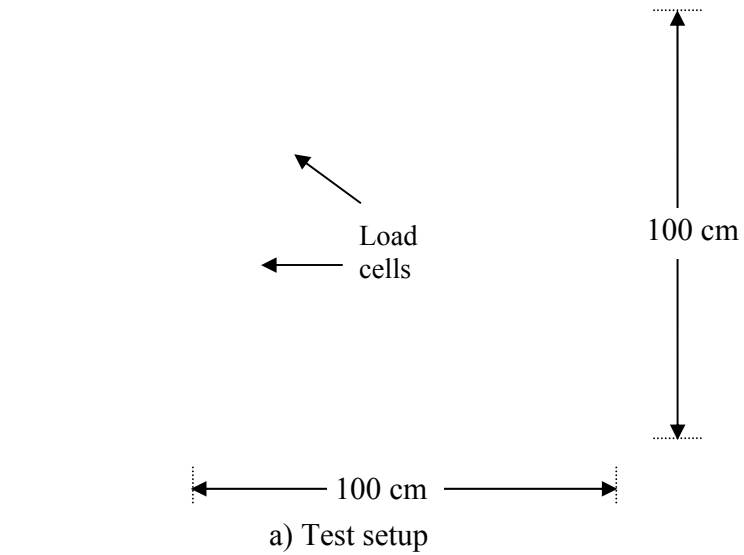


a) Test setup



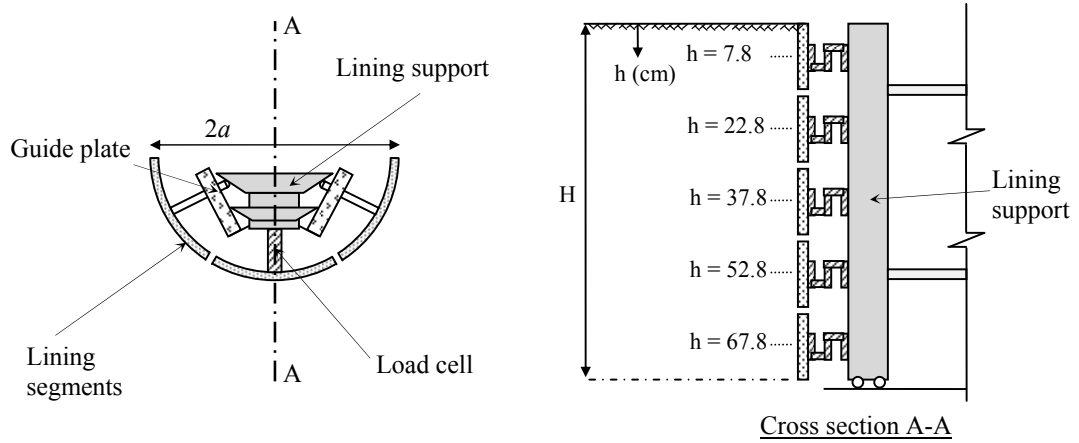
b) Earth pressure distribution

Fig. 6. Semi-cylindrical model shaft and earth pressure distribution for smooth and rough walls (Adapted from Fujii et al., 1994)

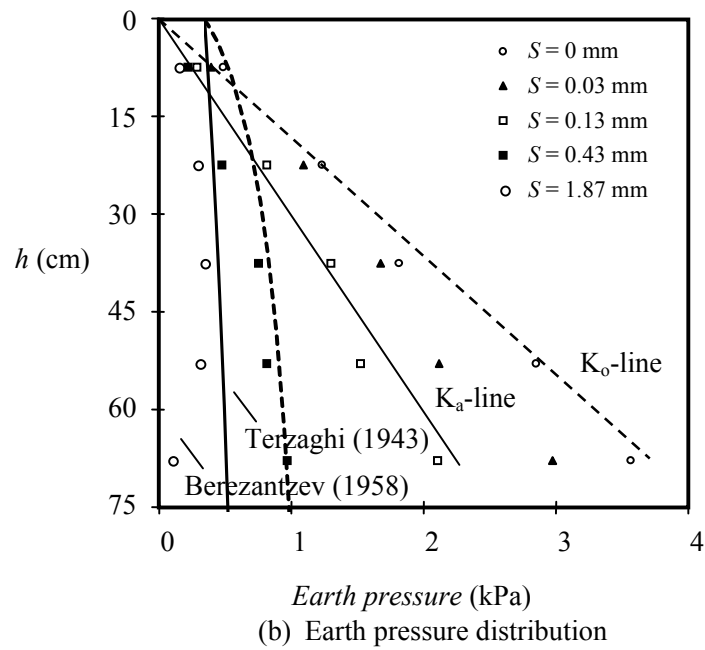


b) Measured earth pressure

Fig. 7. Quarter-cylinder model shaft and the earth pressure distribution (Adapted from Herten & Pulsfort, 1999)

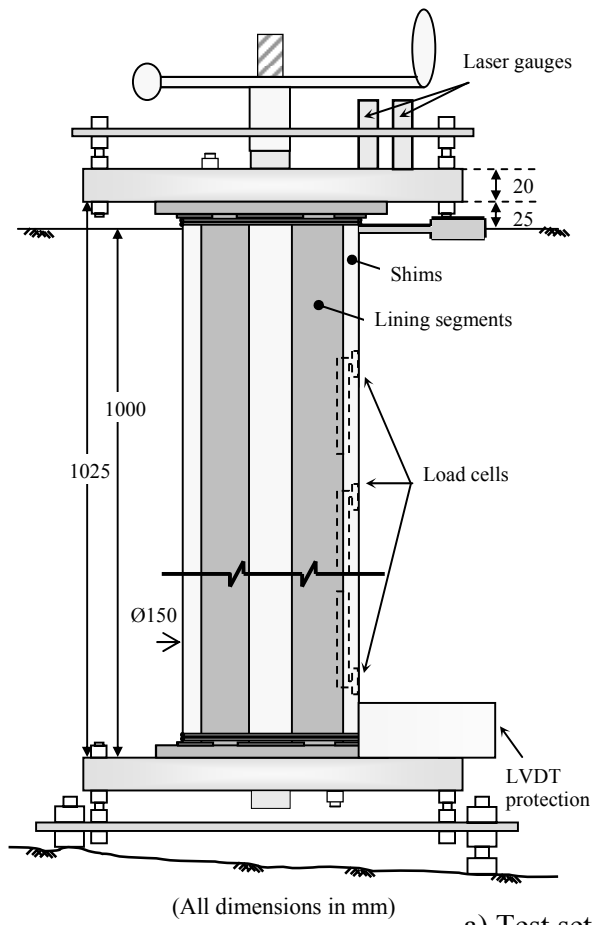


(a) Schematic of the shaft apparatus



(b) Earth pressure distribution

Fig. 8. Semi-cylindrical model shaft and the measured earth pressure using a shape aspect ratio, H/a , of 4.286 (Adapted from Chun & Shin, 2006)

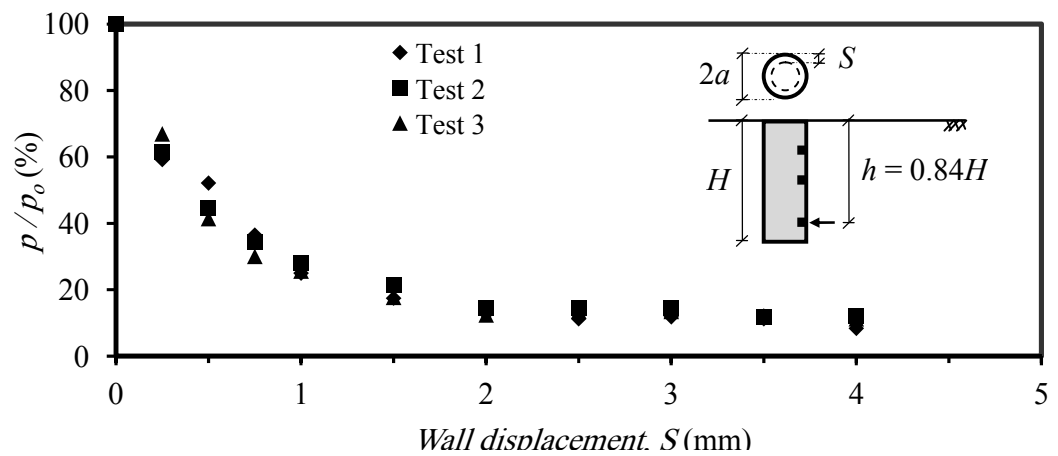


a) Test setup

Lining segment



Details of the end section



b) Normalized pressure at $h = 0.84H$

Fig. 9. Details of the full axisymmetric shaft apparatus and the measured results (Tobar & Meguid, 2009)